Fetal MR Imaging: An Overview

Xianyun Cai[1]; Xin Chen[1]; Cong Sun[1]; Tuantuan Wang[1]; Hong Tang[1]; Jinxia Zhu[2]; Guangbin Wang[1]

[1]Department of MR, Shandong Medical Imaging Research Institute, Shandong University, China
[2]Siemens Healthineers, MR Collaboration, Beijing, China

The primary objective of prenatal diagnosis is to obtain genetic, anatomical, biochemical, and physiological information about the fetus that will allow the detection of any abnormalities that may have implications for the fetal and postnatal periods. This will make it possible to offer the family information, genetic counseling, and therapeutic alternatives. The main imaging method used for routine fetal examinations is ultrasonography (US). It is noninvasive, inexpensive, widely available, and can provide real-time studies without ionizing radiation. However, in cases of advanced gestational age, patient obesity, oligohydramnios, improper fetal position, and interposition of intestinal gas or pelvic acoustic shadows, US might have technical limitations and be unable to confirm findings. In our department, we consider using MRI when the US findings are equivocal or when the US images are difficult to interpret due to factors such as late pregnancy or an inaccessible fetal position. Fetal MR imaging[1] is regarded as a valuable adjuvant imaging tool for dedicated cases at field strengths of 3T or less. In general, with appropriate sequence adaptations, examinations of the fetus at 3T are comparable with images obtained at 1.5T. Also, because of the higher image resolution and signal-to-noise ratio (SNR), finer structures and lesions can be delineated at 3T. However, a major drawback is that examinations at 3T are more prone to artifacts, which complicates imaging the fetus for traditional referrals (maternal obesity, polyhydramnios). It is therefore important to decide which system might be better suited to address certain indications [1]. Investigation of normal organ development with fetal MRI has been described by Prayer et al. [2]. Maturational processes in utero are characterized by changes in the shape, size, and content/composition of organs, and by their relationship to each other.

In our institution, all the MRI examinations were performed on a 1.5T MAGNETOM Amira (Siemens Shenzhen Magnetic Resonance, Shenzhen, China) with spine and body array coils positioned over the lower pelvic area. Since our department introduced fetal MRI in June 2006, a total of 15,000 pregnant women with various anomalies (screened by ultrasonography) have been referred for fetal MRI examinations at our institution. The cases include brain, spine, chest, and abdominal anomalies. A placental MRI scan was performed for the first time in 2009, and 1,102 such scans have been performed to date. A total of 235 fetal spine scans have been performed since 2015, when susceptibility-weighted imaging (SWI) – a technique developed by Siemens [3], which conventionally uses the BOLD mechanism to generate venograms of the brain and to quantify venous oxygenation levels [4] – was first modified for fetal spine imaging with fast data acquisition by Robinson et al. [5]. In recent years, the development of MR sequences has led to major changes in fetal MRI imaging in our unit.

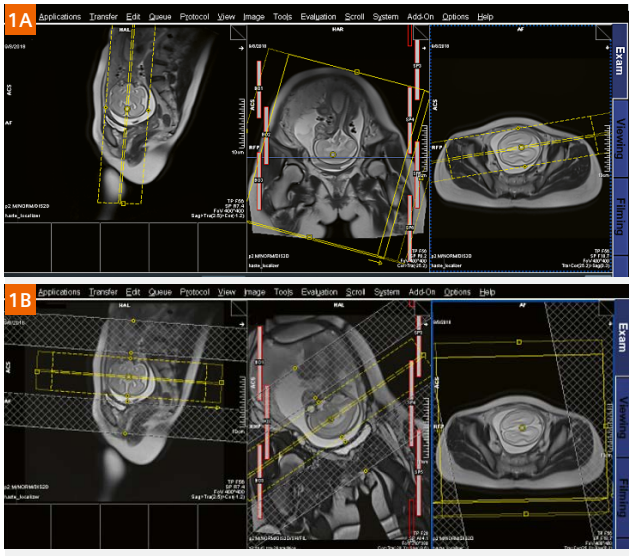

Figure 1:
Sagittal and coronal localizer images of the fetal brain.

[1]*Siemens Healthineers disclaimer does not represent the opinion of the authors: MR scanning has not been established as safe for imaging fetuses and infants less than two years of age. The responsible physician must evaluate the benefits of the MR examination compared to those of other imaging procedures.*

The rise and development of fetal magnetic resonance imaging

Origins

Since fetal MR imaging was first used in 1983 [6], no consistent or convincing evidence has emerged to suggest that briefly exposing a fetus to the changing electromagnetic fields of MR imaging has any harmful effects. In the early days, however, the acquisition time was too long and the motion artifacts were severe, which resulted in poor image quality and hindered the development of fetal MRI. With the development of ultrafast sequences in the 1990s, such as single-shot steady-state free precession (SSFP), half-fourier acquisition single-shot turbo spin echo (HASTE), fast T1-weighted gradient echo, and echo planar imaging, MR imaging became a noninvasive modality that could complement US in detecting fetal abnormalities, establishing prognoses, and assisting in perinatal management.

Safety

With fetal MRI, safety considerations such as exposure times, gradient field switching, noise, and radiofrequency power deposition should be kept in mind while following established guidelines [5–9]. No documented indications exist for using contrast agents in fetal MR imaging. Generally speaking, fetal MR imaging should be avoided in the first trimester, since the fetal cells are rapidly dividing and differentiating, and the influence of MRI on organogenesis is still unclear. Also, it is difficult to obtain good-quality images in very young fetuses.

Another important issue to consider in fetal MRI concerns gadolinium-based intravenous contrast media. These agents have been shown to cross the placenta and may appear in the fetal bladder, which means they are reabsorbed from the amniotic fluid by swallowing. The use of gadolinium-based contrast agents for MR imaging in pregnant women remains controversial. Recently, an animal experiment was conducted to determine whether gadolinium remains in juvenile nonhuman primate tissue after maternal exposure to intravenous gadoteridol during pregnancy. The study concluded that gadoteridol could cross the placenta. Given the similarities between human and nonhuman primate placental physiology, the study suggests there could be relatively little deposition in human fetal tissues after maternal gadoteridol injection. However, the long-term risk of such low levels of gadolinium deposition is still unknown. At our institution, no intravenous injection (of gadolinium agents or sedation agents) was used for any of the examinations, and specific absorption rate limits were in keeping with departmental protocols.

Moreover, maternal indications for prenatal MRI also need to be taken into account.

Fetal MR imaging

All the patients were imaged in supine or left-lateral position, depending on what was most comfortable. Fetal images are obtained in three orthogonal planes in the mother to plan the sagittal, coronal, and axial views of the fetus. The last sequence is used as a reference for planning the next sequence to compensate for fetal movement. All sequences are performed in all three planes through the fetus. Additional imaging planes, such as oblique sagittal or coronal positions, were obtained as needed. An axial T2-weighted sequence may be performed through the fetal brain for purposes of gestational dating. In recent years, ultrafast MR imaging sequences have provided short image acquisition times and usually prevent fetal motion from degrading image quality.

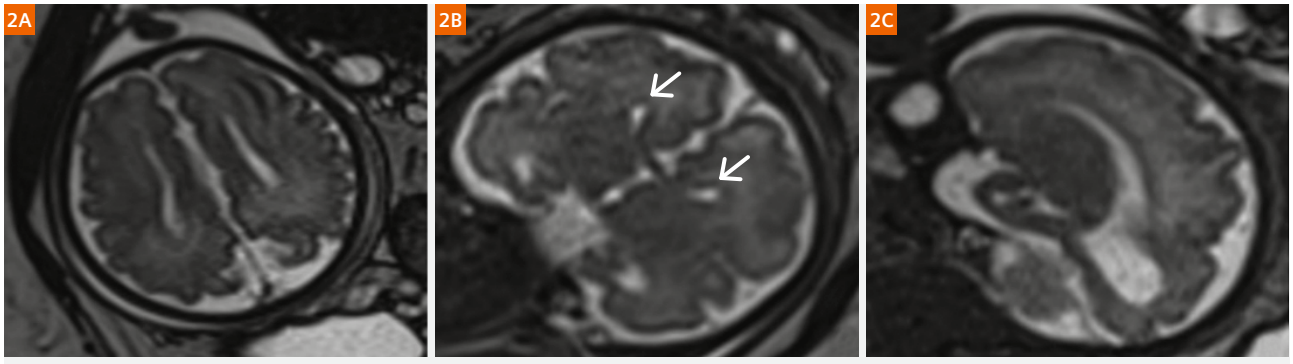

Figure 2: Corpus callosum agenesis
Sagittal HASTE **(2C)** shows complete absence of the corpus callosum. Axial TrueFISP **(2A)** shows parallel orientation of lateral ventricles. Coronal TrueFISP **(2B)** shows steer-horn-shaped frontal horns (arrows) resulting from the impression of Probst bundles.

1. **T2-weighted sequences**
   T2-weighted imaging (T2WI) includes single-shot, and half-Fourier single shot turbo spin echo (SSTSE, HASTE) T2-weighted sequences, and balanced sequences such as true fast imaging with steady-state precession (TrueFISP), which produces high tissue contrast and highlights the hyperintense amniotic fluid. At our institution, T2 HASTE and T2 TrueFISP were the most frequently used sequences for evaluating fetal anatomy. The TrueFISP sequence also allows vascular studies that require no intravenous contrast agent and can reveal hyperintense fetal vessels (vessels appear hypointense on SSTSE T1-weighted and T2-weighted images).

2. **T1-weighted sequences**
   T1-weighted imaging (T1WI), including 3D dual gradient echo (GRE), 2D fast spoiled GRE (FISP), and 3D liver acquisition and volume acquisition (3D VIBE), show less tissue contrast than T2WI sequences. T1WI sequences are primarily used to identify subacute bleeding, calcification, and lipoma, which appear as hyperintense loop structures in studies of congenital diaphragmatic hernia (CDH). T1WI sequences are also used to assess the presence and distribution of meconium, which enables accurate diagnosis of gastrointestinal abnormalities, reveals the size and location of the fetal liver, and can identify fetal, placental, or maternal hemorrhage.

3. **Susceptibility-weighted imaging**
   Susceptibility-weighted imaging (SWI) uses the intrinsic nature of local magnetic fields to enhance image contrast and thereby improve the visibility of various susceptibility sources and facilitate diagnostic interpretation [7]. It is worth mentioning that calcification is strongly diamagnetic and therefore decreases the magnetization in bone compared to the applied magnetic field. The technique results in a high contrast between bone and soft tissue, but a low contrast between different types of soft tissue. The low-signal bone is therefore easily distinguishable from the surrounding soft tissue.

4. **Diffusion-weighted imaging**
   As well as being used to diagnose cerebral infarction, diffusion-weighted imaging (DWI) sequences are currently being developed for fetal applications. The technique is already being used to study the maturity of lung parenchyma.

Fluid-sensitive short T1 inversion recovery (STIR), intravoxel incoherent motion imaging (IVIM), MR hydrography, and other sequences are not part of the routine fetal protocol but may be performed in specific cases where necessary.

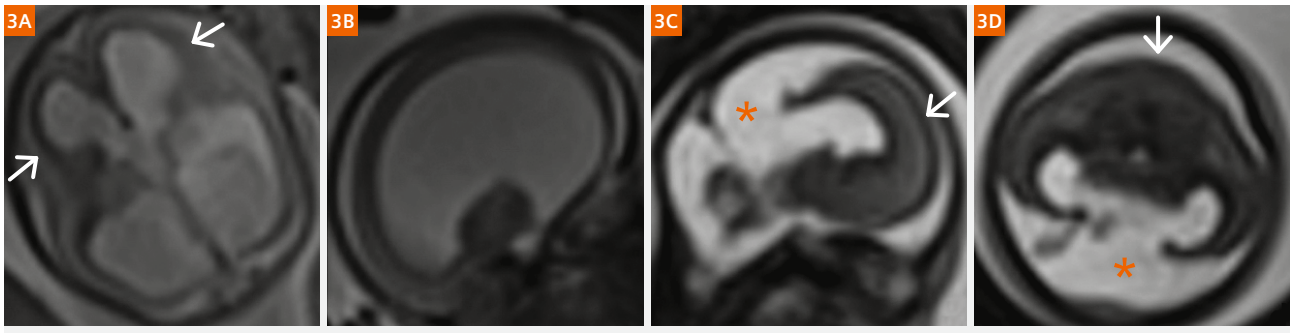

Figure 3: Severe hydrocephalus (3A, B) and alobar holoprosencephaly (3C, D)
Axial and coronal **(3A)** T2 HASTE imaging shows the marked dilation of the cerebral bilateral ventricle stenosis with only a thin mantle of overlying cerebral cortex (arrows). Sagittal **(3C)** and coronal **(3D)** T2 TrueFISP imaging shows only minimal frontal cerebral mantle (white arrows in 3A and B) and replacement of the majority of the brain with CSF (star). Coronal **(3C)** and axial **(3D)** T2 TrueFISP show a complete absence of falx, an interhemispheric fissure, and corpus callosum. Also visible is a horseshoe-shaped monoventricle communicating with a dorsal cyst (star).

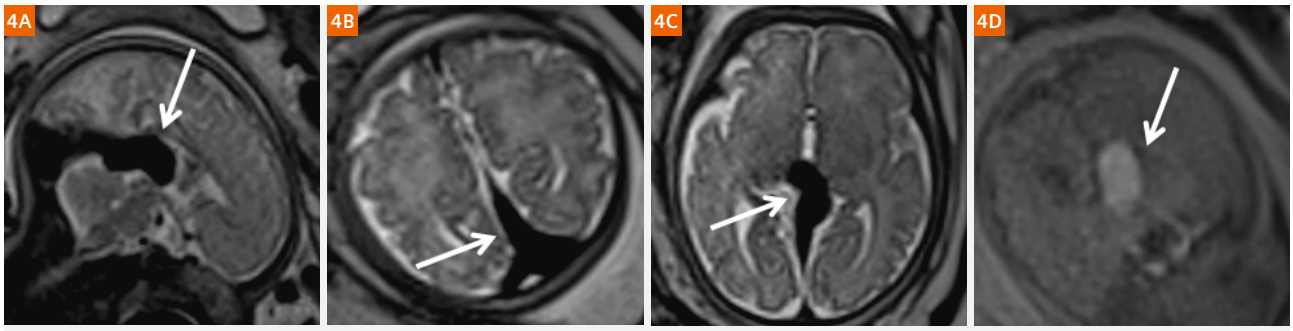

Figure 4: Galen vein malformation
Sagittal **(4A)** and coronal and axial **(4B)** T2 HASTE show a large varix (arrow) replacing the Galen vein, which exhibits hyperintensity on T1WI (**4D**, arrow).

The anatomy and anomalies in fetal MRI

Brain and spine

Imaging the central nervous system (CNS) anatomy and relevant pathology is clinically important for the early identification of cranial and spinal malformations and anomalous development. Fetal MRI has been shown to have higher contrast resolution and SNR than ultrasonography when it comes to illustrating the morphological changes in cranial and spinal brain abnormalities [8]. Most of the literature describing the results of MRI in large series of fetuses with CNS abnormalities deals with cerebral pathology. Spinal anomalies are usually described using examinations of smaller groups of patients or in case reports.

MR images of the developing fetal brain reflect changes in histogenesis and myelination. Subsequent changes are seen in the brain volume, surface configuration (sulcation), and internal configuration. Detailed information provided by MRI is necessary to evaluate the differentiation of white and gray matter, migration and myelination disorders, brain morphology and pathologies, and cranial posterior fossa and midline structures. Here, localizer brain scans (Fig. 1) provide the basis for images demonstrating different developmental deformities (Figs. 2–4).

The spinal canal and cord anomalies are among the CNS abnormalities which occur as a result of disruptions in formation and maturation. During the first three to five weeks of gestation (neurulation period), the neural tube, notochord, spine, and cranium develop. Disorders that occur at this stage of gestation (i.e., most spinal canal defects) are called "dorsal induction abnormalities". The dysraphic spinal canal and spinal cord disorders are divided into three groups: open dysraphic abnormalities, occult dysraphic abnormalities, and latent dysraphic abnormalities (e.g., diastematomyelia, hydromyelia, syringomyelia, dorsal dermoid sinus, teratoma, hamartoma, lipoma, dermoid/epidermoid cyst, and caudal regression syndrome).

Congenital anomalies of the spine occur at four to six weeks of gestation due to abnormal vertebral development that causes asymmetric growth of the spine. Anomalies in the ossification center of the fetal vertebral body result in bony defects such as hemivertebrae, butterfly vertebrae, and block vertebrae, which cause congenital scoliosis. MRI of fetuses diagnosed with osseous anomalies of the spine remains largely unexplored. Recently, we adapted and improved a clinically available SWI sequence for fetal spine imaging to evaluate vertebral malformations and anomalous vertebral development (in bony structures). We also typically used T2 TrueFISP and HASTE sequences to evaluate the recognition of the fetal spinal canal and spinal cord pathologies, as described in previous studies [9].

For MR imaging of the fetal spine, the protocol first involved a scout imaging sequence to gather information about the orientation of the fetus. Subsequent routine clinical sequences included T1WI, DWI, HASTE, T2-weighted TrueFISP, and SWI sequences. The HASTE, TrueFISP, and SWI sequences were obtained in the axial, coronal, and sagittal planes. The axial plane is best for assessing the neural arches, the coronal plane allows an additional assessment of the ribs and of pedicular widening in cases of spina bifida, and the sagittal plane is best for assessing the whole spine lengthways. The SWI sequence is best run immediately after routine HASTE or TrueFISP sequences, depicting the required anatomy by simply copying the slice parameters and thereby minimizing the time between sequences and reducing the chance of fetal motion. Here, localizer spine scans (Fig. 5) provide the basis for demonstrating various developmental deformities as follows (Figs. 5–9).

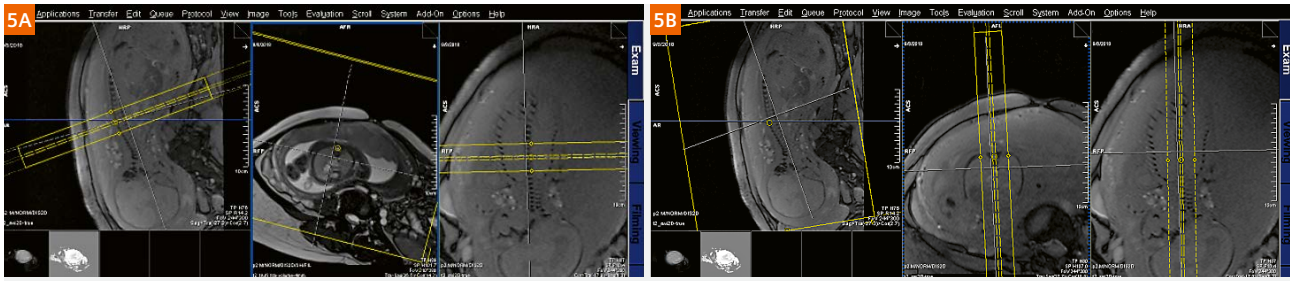

Figure 5:
Axial, sagittal, and coronal localizer images of the fetal spine.

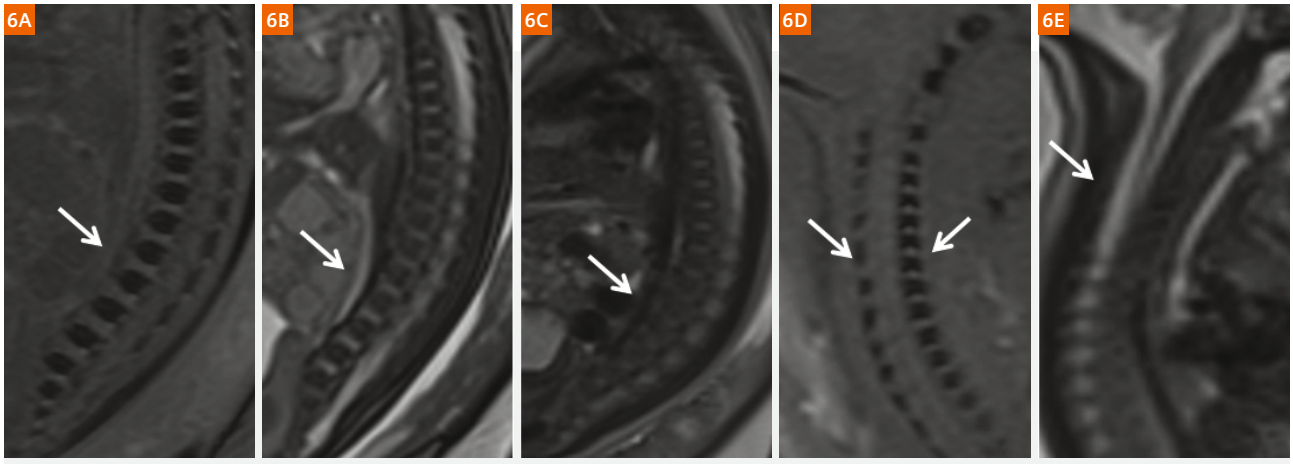

Figure 6:
Images at 32 weeks' gestation (6A–C) and 26 weeks' gestation (6D–E) with normal fetal spine structures. Sagittal view of the thoraco-lumbar spine, MR images including SWI (6A), TrueFISP (6B), and HASTE (6C). The SWI **(6A, D)** clearly shows the vertebral bodies and the posterior elements (arrows). On a similar plane in the same position using TrueFISP **(6B, E)** and HASTE **(6C)**, the vertebral column (arrows) is shown poorly but could reveal the structures of the intraspinal canal.

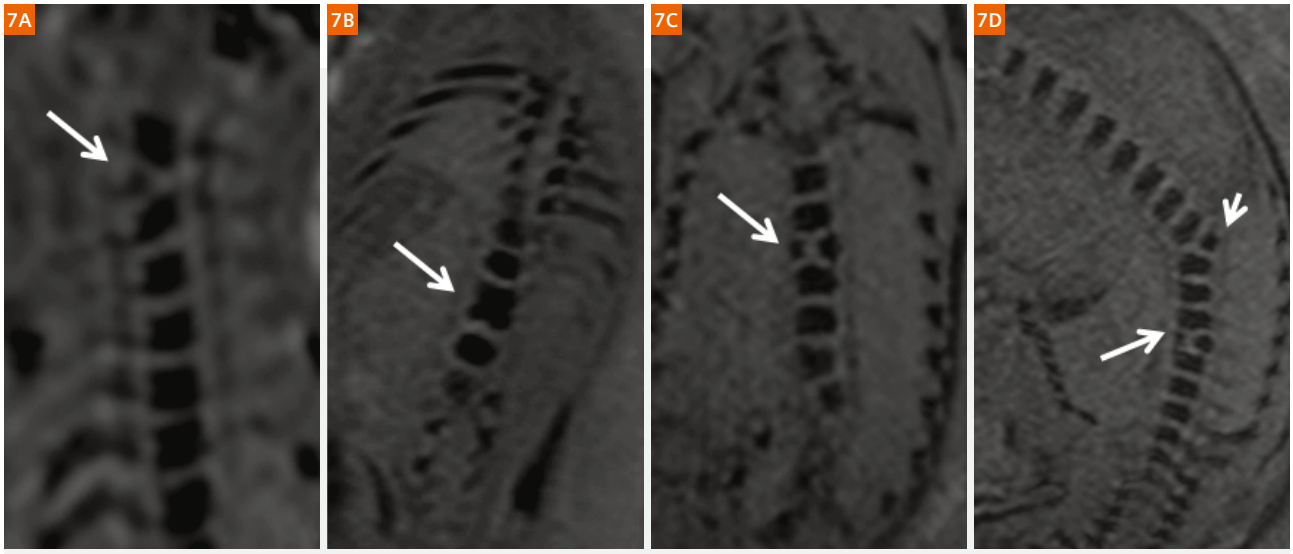

Figure 7:
SWI images at 26 weeks' gestation (7A), 25 weeks (7B), 33 weeks (7C), and 34 weeks with fetal vertebral anomalies. Coronal views of the cervical **(7A)**, lumbar **(7B)**, and thoracic **(7C)** spine show hemivertebrae, block vertebrae, and butterfly vertebrae. Multiple vertebral anomalies with hemivertebrae (short arrows) and butterfly vertebrae (long arrows) are clearly visible in coronal 2D SWI **(7D)**.

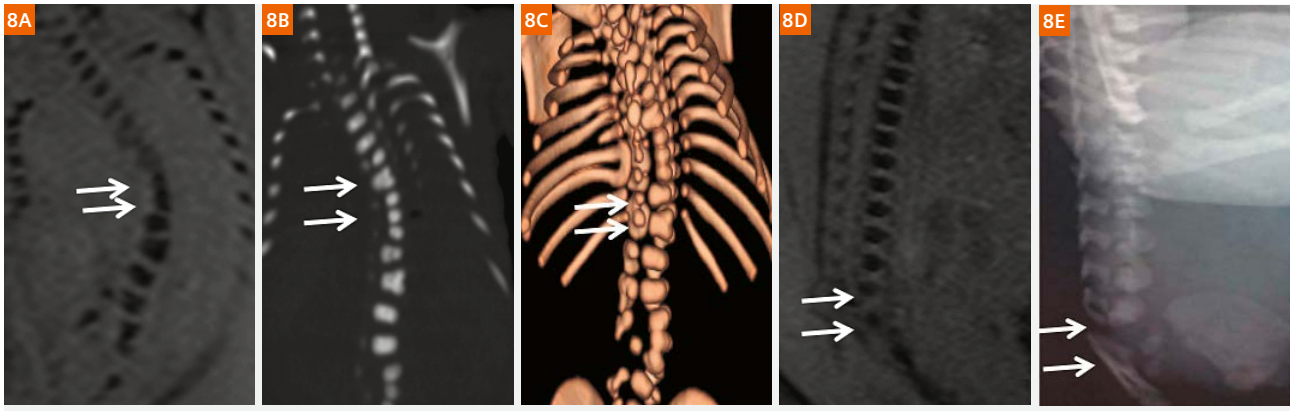

Figure 8:
Images at 24 weeks' gestation (8A–E) with multiple vertebral anomalies (8A–C) and at 32 weeks' gestation (8D–E) with caudal regression syndrome. SWI **(8A)** shows multiple vertebral anomalies (arrows) that were consistent with the postmortem CT (**8B**, **C**, arrows). SWI shows dysplasia of the sacrococcygeal vertebrae (arrows) that was consistent with the postmortem X-ray (**8E**, arrows).

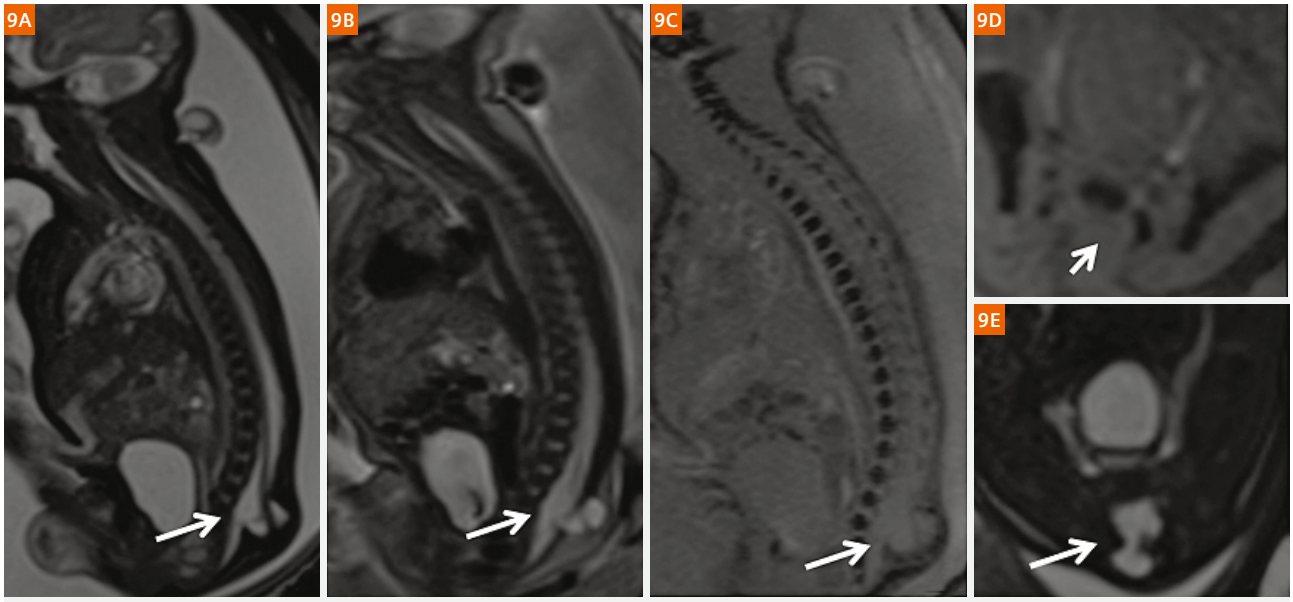

Figure 9:
Images at 32 weeks' gestation with spinal dysraphism (9A–E). Sagittal view of the MR images include HASTE **(9A)**, TrueFISP **(9B, E)**, and SWI **(9C, D)**. The pocket-like processes protruding from the sacrococcygeal spinal canal were all visible, and the spinal cord was found to extend from the spinal canal to the dilated dural capsule (9A, B, E, long arrow), which could not be seen with SWI (9C, D). However, SWI showed excellent osseous spinal structures and demonstrates the pedicular widening (9C, long arrow; 9D, short arrow).

Chest

At present, ultrasound and MRI are the only diagnostic tools that can examine fetal lungs noninvasively. MRI provides additional biochemical and functional information that cannot be obtained by ultrasound as well as detailed structural information. This therefore makes it a valuable diagnostic adjunct for assessing fetal lung development [10]. Congenital chest malformations can range from small and asymptomatic entities to large, space-occupying masses that require immediate surgical treatment. An understanding of fetal chest masses is essential for appropriate monitoring during pregnancy, and for treatment recommendations and delivery management. The most common congenital chest anomalies include congenital cystic adenomatoid malformation (CCAM), congenital diaphragmatic hernia (CDH), bronchopulmonary sequestration (BPS), congenital hydrothorax, and congenital lobar emphysema. Less common entities include congenital high airway obstruction syndrome (CHAOS), congenital bronchogenic cyst, bronchial atresia, pulmonary arteriovenous malformation (PAVM), congenital pulmonary lymphangiectasia, pulmonary hypoplasia-aplasia, mediastinal teratoma, and mediastinal lymphangioma. These pulmonary abnormalities are not mutually exclusive; they frequently occur together as hybrid conditions.

The MRI sequences used to evaluate the fetal chest include HASTE, fast single-shot echo, and TrueFISP. In our unit, HASTE and TrueFISP images are the most useful for evaluating the lung anatomy. The lungs typically contain a significant amount of alveolar fluid, which is homogeneously hyperintense relative to the chest wall muscle on T2-weighted images.

Congenital diaphragmatic hernia and extralobar pulmonary sequestration were demonstrated as follows (Figs. 10, 11).

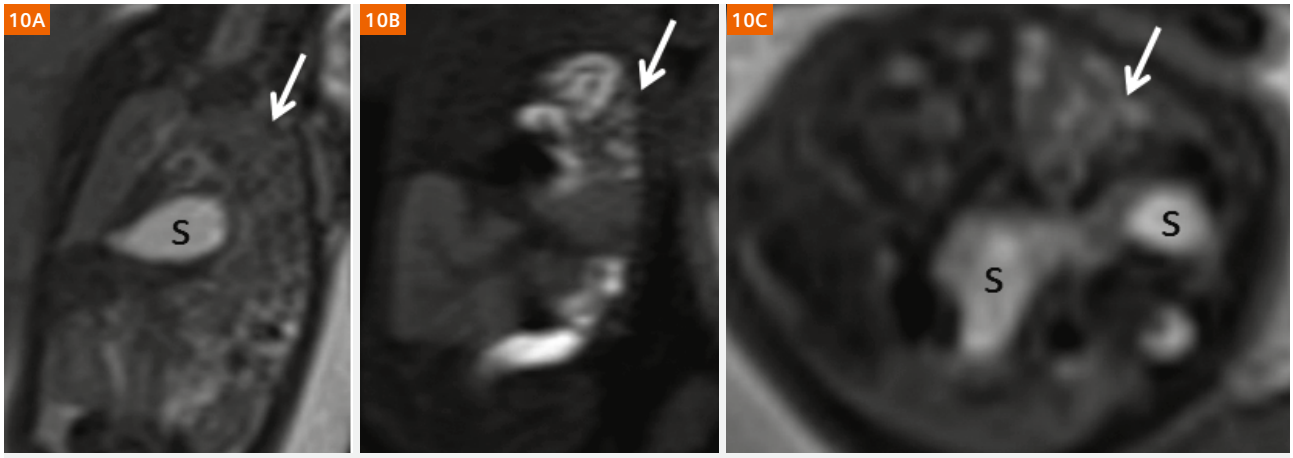

Figure 10: Congenital diaphragmatic hernia at 28 weeks' gestation
Coronal **(10A)** and axial **(10C)** T2 HASTE, and T1w imaging **(10B)** show herniated content (arrow) displacing the heart and compressing the unilateral lung and portions of the bowel (10B, arrow) and stomach (S) occupying the unilateral hemithorax.

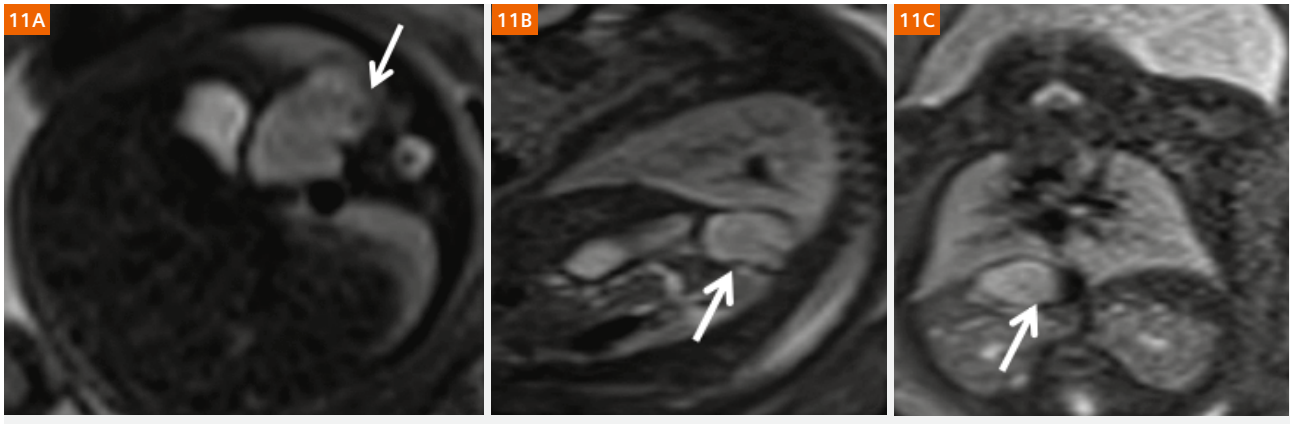

Figure 11: Extralobar pulmonary sequestration at 32 weeks' gestation
Axial **(11A)**, sagittal **(11B)**, and coronal **(11C)** T2 HASTE show a homogeneous, high T2WI signal between the left subphrenic space and left kidney with a clear boundary (arrow). Postnatal CT (not shown) enhancement shows a vascular shadow connected to the aorta.

Abdominal abnormalities and tumors

Fetal abdominal deformities and tumors vary in their location, and can be derived from the gastrointestinal tract, liver, kidney, and retroperitoneum. Congenital tumors are defined as those that are present during the fetal stage or at birth. In some cases, MRI can provide important information and even add important findings to prenatal US for perinatal management by visualizing fetal tumors with common tumor-related complications and other exceptional congenital abnormalities [11]. Common indications for fetal gastrointestinal (GI) MRI include suspected esophageal, small bowel, and large bowel obstruction, bowel malrotation, and bowel perforation resulting in meconium peritonitis or meconium pseudocyst. MRI is also particularly useful for evaluating rare GI abnormalities, such as megacystis microcolon intestinal hypoperistalsis syndrome (MMIHS), cloacal exstrophy, and cloacal malformation. Although US remains the modality of choice for investigating fetal anomalies, the findings are often nonspecific and may relate to transient normal variants [12]. In addition, urine and fluid in the colon beyond 24 weeks may have a similar sonolucent appearance on US and opposite appearances on MR images, allowing better identification and discrimination. In our department, a T1-weighted breath-hold sequence is completed in the coronal plane and, if necessary, in the sagittal and axial planes.

Different developmental deformities in the abdomen were demonstrated as follows (Figs. 12–16).

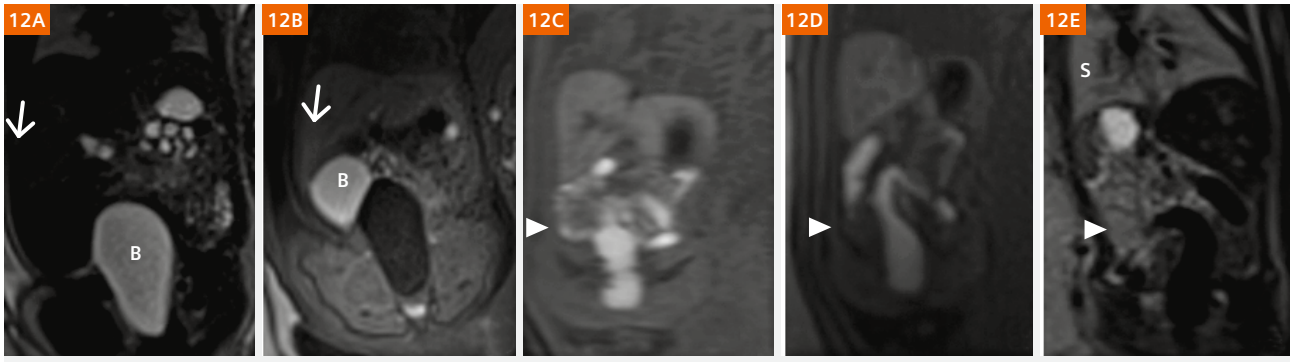

Figure 12: Localized intestinal dilatation at 30+4 weeks' gestation, and imperforate anus at 28 weeks' gestation
Coronal T2 HASTE **(12A)** and T1w **(12B)** images show the dilated loops of one part of the gastrointestinal tract. It is markedly hyperintense on T1WI (arrow) and hypointense on T2WI (arrow). Coronal T1WI **(12C, D)** and T2 TrueFISP **(12E)** images show a prominent rectum (arrowhead) with high T1 signal intensity and low T2 signal intensity. The abnormality of the large bowel was identified and diagnosed as rectal atresia during a postnatal physical examination. B = urinary bladder, S = stomach

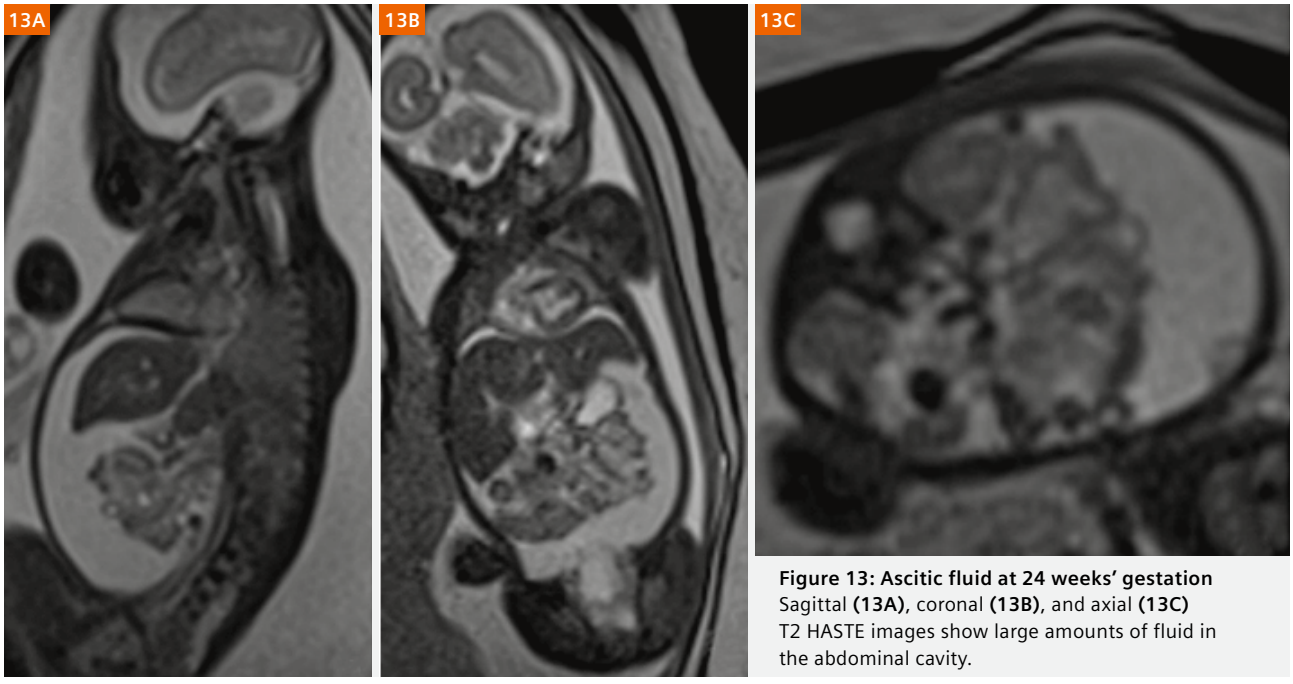

Figure 13: Ascitic fluid at 24 weeks' gestation
Sagittal **(13A)**, coronal **(13B)**, and axial **(13C)** T2 HASTE images show large amounts of fluid in the abdominal cavity.

Figure 14: Neuroblastoma at 28 weeks' gestation
Axial **(14A)**, sagittal **(14B)**, and coronal **(14C)** T2 HASTE images show a solid mass with a clear boundary above a lateral kidney that is hyperintense on a T2-weighted sequence (arrow) and was found to be neuroblastoma after birth.

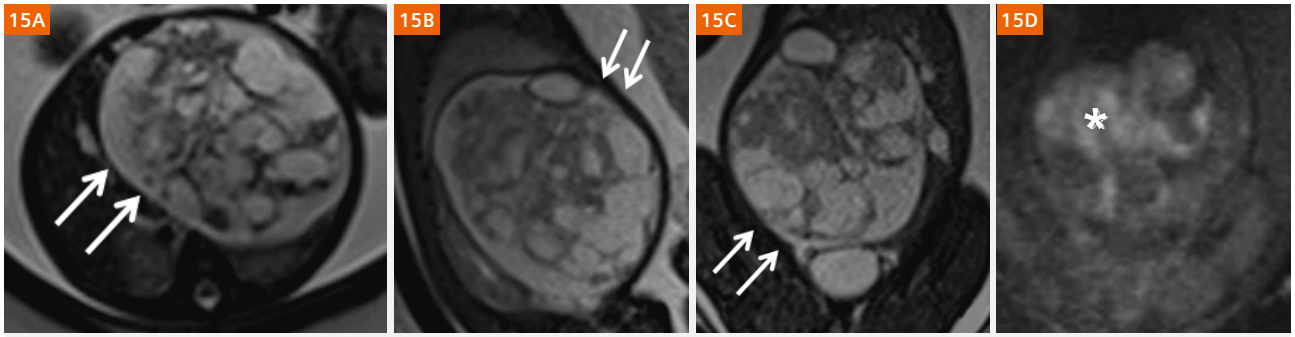

Figure 15: Teratoid tumors at 30 weeks' gestation
Axial T2 HASTE **(15A)**, sagittal **(15B)**, and coronal **(15C)** T2 TrueFISP images show a heterogeneous solid cystic mass with a high-intensity heterogeneous signal (arrows), and surrounding tissue that was markedly squeezed. The giant lesions showed restricted diffusion with DWI (**15D**, star). A histopathological diagnosis of teratoid tumors was made after birth.

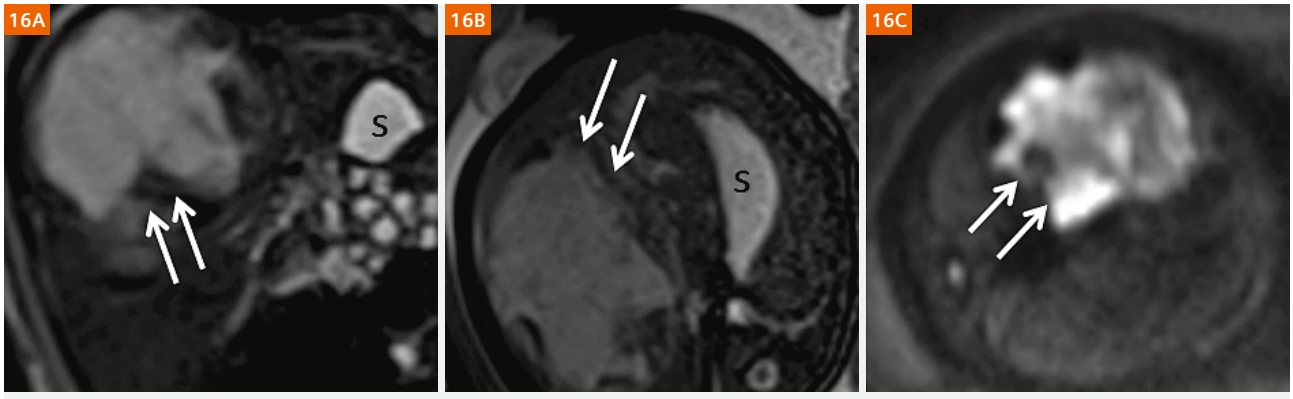

Figure 16: Hepatic hemangioendothelioma at 32 weeks' gestation
Coronal T2 HASTE **(16A)** and axial T2 TrueFISP **(16B)** images show a large heterogeneous and high-signal mass in the liver parenchyma, and highly restricted diffusion with DWI **(16C)**. A histopathological diagnosis of hepatic hemangioendothelioma was made after birth.

Maternal indications for prenatal MRI

In addition to fetal indications, there are several maternal indications for prenatal MR imaging. They include the possibility of uterine rupture, the need to differentiate between placenta accreta and percreta, a large myoma interfering with the pregnancy, and MR pelvimetric measurements. In our unit, the technique of placental MRI and the diagnostic level are increasingly convincing and compelling.

Abnormal invasive placenta (AIP) is a disease with a spectrum of severity characterized by abnormal, firmly adherent placental implantation into the uterus at varying depths. It is typically referred to as placenta accreta, increta, and percreta [13]. When AIP occurs, the placenta may not be completely separated from the uterus at the time of delivery, resulting in potentially life-threatening intrapartum or postpartum massive hemorrhage and associated morbidity such as multisystem organ failure, disseminated intravascular coagulation, and even death. Placenta percreta (PP) is the most dangerous type of AIP. It is characterized by trophoblasts fully penetrating the myometrium and in some cases extending to or breaching the serosa and even invading surrounding structures [14]. An accurate prenatal diagnosis of PP is therefore imperative.

In 2017, our team published an article on placenta accreta [15] that aimed to identify specific MRI features for differentiating PP from placenta accreta (PA), and to characterize the features of invasive placenta previa. Our studies showed a series of MRI features, including myometrial thinning, interrupted myometrium, loss of the placental-myometrial interface, marked placental heterogeneity, dark intraplacental bands, abnormal intraplacental vascularity, abnormal uterine bulge, placental bulge (type I and type II, Fig. 2), uterine serosal hypervascularity, bladder wall nodularity, and extrauterine placental extension. Our results suggest that type II placental bulge and uterine serosal hypervascularity are useful MRI features for differentiating PP from PA. Profoundly abnormal vessels are associated with greater blood loss during caesarean section. Our results could contribute to accurate prenatal diagnosis of PP and help minimize the risk of massive hemorrhage [15].

In our center, all the patients with suspected invasive placenta previa (IPP) were imaged in the supine or left-lateral position with bladders moderately full. T2-weighted HASTE and T2-weighted TrueFISP images were obtained without breath-hold in the axial, coronal, sagittal, and oblique sagittal planes. Additional imaging planes perpendicular to the placenta-uterus interface or uterus-bladder interface were obtained in the region of the suspected AIP.

Several placenta increta and placenta percreta were demonstrated as follows (Figs. 17–20).

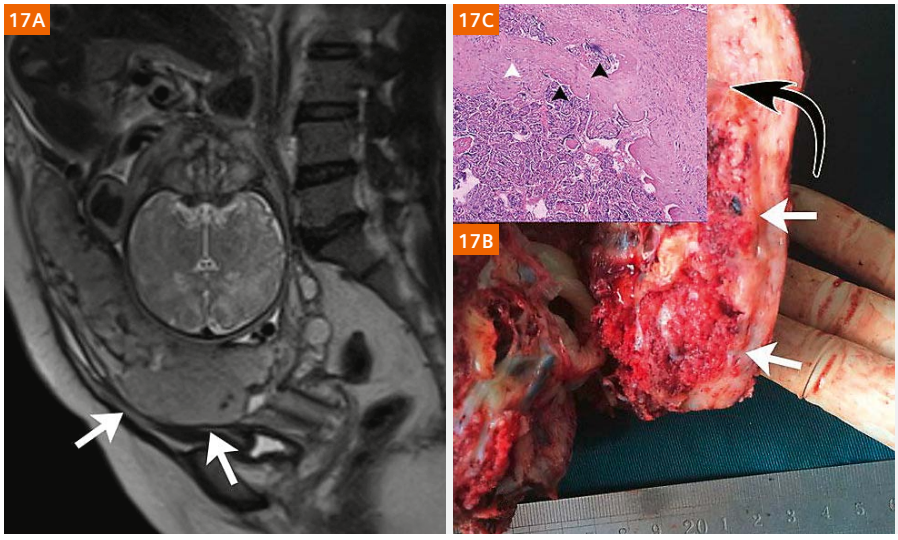

Figure 17: Placenta increta (PI) in a 40-year-old woman at 35 weeks' gestation
A sagittal T2 HASTE MR image **(17A)** demonstrates type I placental bulge (white arrows) with an intact uterine outline. A photograph **(17B)** of gross specimens after hysterectomy shows that the placenta has invaded the myometrium (white arrows) with intact uterine serosa, consistent with PI. A photomicrograph (**17C**, magnification x 400, hematoxylin and eosin stain) shows chorionic villi (black arrowheads) implanted in the myometrium (white arrowhead), consistent with PI.

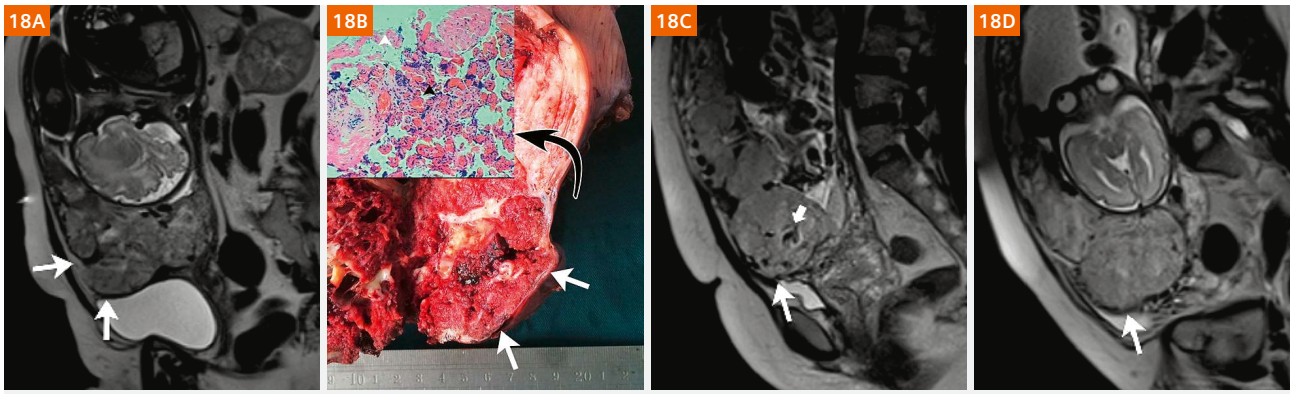

Figure 18: Placenta percreta (PP, 18A, B) in a 39-year-old woman at 30 weeks' gestation
A sagittal T2 HASTE MR image **(18A)** shows type II placental bulge (white arrows) protruding from the uterine outline. A photograph **(18B)** of gross specimens after hysterectomy shows placental invasion (white arrows) through the uterine wall, consistent with PP. A photomicrograph (magnification: x 400, hematoxylin and eosin stain) shows chorionic villi (black arrowhead) penetrating the myometrium (white arrowhead), consistent with PP. Sagittal T2 HASTE MR images show a type IIa placental bulge (long arrow, a focal outward bulge protruding from the uterine outline) with bridging vessels (short arrow) in a 31-year-old woman at 35 weeks' gestation with PP **(18C)** and type IIb placental bulge (long arrow) without bridging vessels in a 29-year-old woman at 32 weeks' gestation with PP **(18D)**.

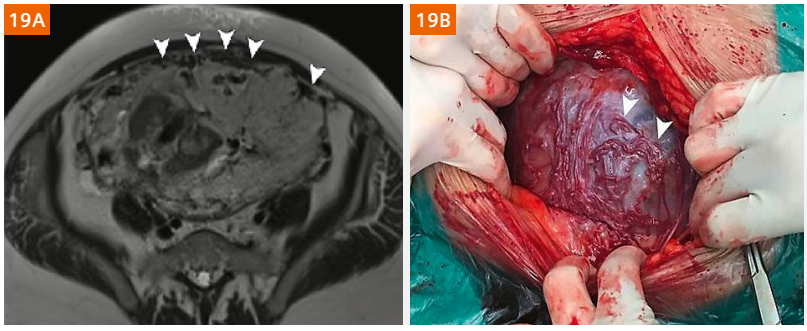

Figure 19: Placenta percreta (PP) in a 35-year-old woman at 29 weeks' gestation
An axial T2 HASTE image **(19A)** shows uterine serosal hypervascularity (arrowheads, tortuous and closely packed vessels along the uterine serosa) in the lower uterine segment.
A photograph **(19B)** taken during cesarean delivery shows the tortuous abnormal vessels in the uterine serosa (arrowheads), consistent with their appearance on MR images.

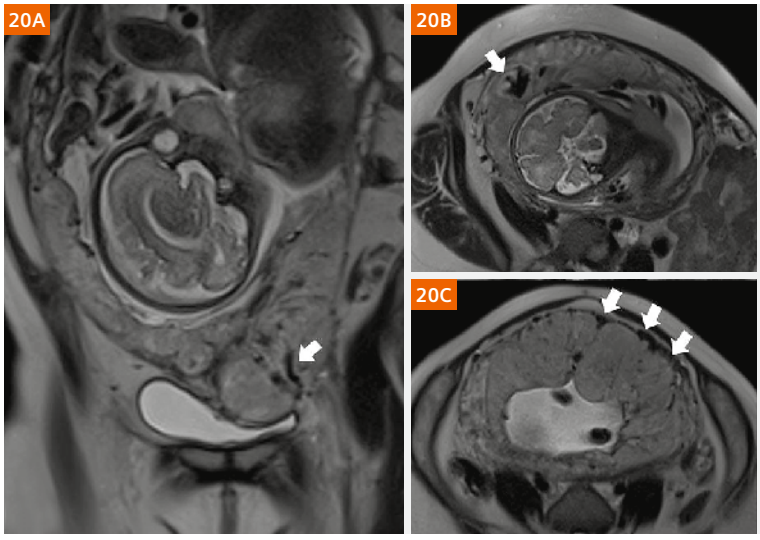

Figure 20:
A coronal T2 HASTE MR image **(20A)** shows bridging vessels (arrow) through the bulging placenta in a 25-year-old woman at 32 weeks' gestation with placenta percreta (PP). An axial T2 HASTE MR image **(20B)** shows abnormal intraplacental vascularity (arrow) in a 28-year-old woman at 30 weeks' gestation with placenta increta (PI). An axial T2 HASTE MR image **(20C)** demonstrates uterine serosal hypervascularity (arrows) in a 34-year-old woman at 35 weeks' gestation with PP.

As outlined in this article, fetal MR imaging is playing an increasingly important role in prenatal diagnostics. Nevertheless, US will and should remain the first choice for prenatal screening due to its low cost, ease of availability, and superb safety profile. Advances in fetal MRI have given clinicians powerful tools to identify fetal pathologies. These can range from small and symptomatic abnormalities to large, space-occupying masses that require immediate surgical treatment. The information obtained with fetal MR imaging can be helpful and allow early planning of prenatal management.

References

1 Weisstanner C, Gruber GM, Brugger PC, et al. Fetal MRI at 3T – ready for routine use? Br J Radiol. 2017; 90(1069):20160362.
2 Prayer D, Brugger PC. Investigation of normal organ development with fetal MRI. Eur Radiol. 2007; 17(10):2458-2471.
3 Haacke EM, Xu Y, Cheng YC, et al. Susceptibility weighted imaging (SWI). Magn Reson Med. 2004; 52(3):612-618.
4 Reichenbach JR, Jonetz-Mentzel L, Fitzek C, et al. High-resolution blood oxygen-level dependent MR venography (HRBV): a new technique. Neuroradiology 2001; 43(5):364-369.
5 Robinson AJ, Blaser S, Vladimirov A, et al. Foetal "black bone" MRI: utility in assessment of the foetal spine. Br J Radiol. 2015; 88(1046):20140496.
6 Smith FW, Adam AH, Phillips WD. NMR imaging in pregnancy. Lancet. 1983; 1(8314-5):61-62.
7 Reichenbach JR, Venkatesan R, Schillinger DJ, et al. Small vessels in the human brain: MR venography with deoxyhemoglobin as an intrinsic contrast agent. Radiology. 1997; 204(1):272-277.
8 Coakley FV, Glenn OA, Qayyum A, et al. Fetal MRI: a developing technique for the developing patient. AJR Am J Roentgenol. 2004; 182(1):243-252.
9 Duczkowska A, Bekiesinska-Figatowska M, Herman-Sucharska I, et al. Magnetic resonance imaging in the evaluation of the fetal spinal canal contents. Brain Dev. 2011; 33(1):10-20.
10 Kasprian G, Balassy C, Brugger PC, et al. MRI of normal and pathological fetal lung development. Eur J Radiol. 2006; 57(2):261-270.
11 Nemec SF, Horcher E, Kasprian G, et al. Tumor disease and associated congenital abnormalities on prenatal MRI. Eur J Radiol. 2012; 81(2):e115-e122.
12 Veyrac C, Couture A, Saguintaah M, et al. MRI of fetal GI tract abnormalities. Abdom Imaging. 2004; 29(4):411-420.
13 Belfort MA. Placenta accreta. Am J Obstet Gynecol. 2010; 203(5):430-439.
14 Silver RM, Barbour KD. Placenta accreta spectrum: accreta, increta, and percreta. Obstet Gynecol Clin North Am. 2015; 42(2):381-402.
15 Chen X, Shan R, Zhao L, et al. Invasive placenta previa: Placental bulge with distorted uterine outline and uterine serosal hypervascularity at 1.5T MRI – useful features for differentiating placenta percreta from placenta accreta. Eur Radiol. 2018; 28(2):708-717.

Contact

Guangbin Wang
Department of MR
Shandong Medical Imaging Research Institute
Shandong University
324, Jingwu Road, Jinan
Shandong 250021
China
wgb7932596@hotmail.com


Guangbin Wang


Xianyun Cai